Inorganic Chemistry

Article

pubs.acs.org/IC

A *trans*-1,2 End-On Disulfide-Bridged Iron–Tetracarbene Dimer and Its Electronic Structure

Steffen Meyer,[†] Oliver Krahe,[‡] Claudia Kupper,[†] Iris Klawitter,[†] Serhiy Demeshko,[†] Eckhard Bill,[‡] Frank Neese,*[,‡] and Franc Meyer*[,†]

[†]Institut für Anorganische Chemie, Georg-August-Universität Göttingen, Tammannstraße 4, 37077 Göttingen, Germany

[‡]Max Planck Institute for Chemical Energy Conversion, Stiftstraße 34–36, 45470 Mülheim an der Ruhr, Germany

Supporting Information

ABSTRACT: A disulfide-bridged diiron complex with [Fe–S–S–Fe] core, which represents an isomer of the common biological [2Fe–2S] ferredoxin-type clusters, was synthesized using strongly σ-donating macrocyclic tetracarbene capping ligands. Though the complex is quite labile in solution, single crystals were obtained, and the structure was elucidated by X-ray diffraction. The electron-rich iron–sulfur core is found to show rather unusual magnetic and electronic properties. Experimental data and density functional theory studies indicate extremely strong antiferromagnetic coupling ($-J > 800$ cm^{-1}) between two low-spin iron(III) ions via the S_2^{2-} bridge, and the intense near-IR absorption characteristic for the [Fe–S–S–Fe] core was assigned to a S → Fe ligand-to-metal charge transfer transition.

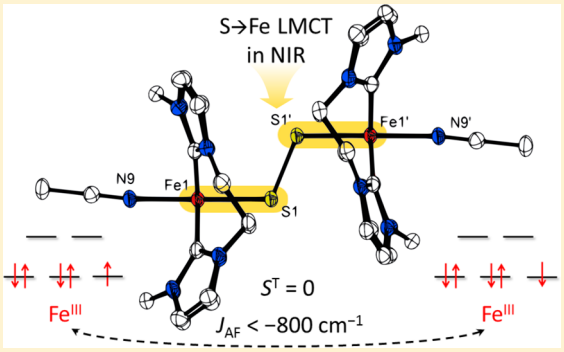

INTRODUCTION

[2Fe–2S] clusters containing a rhombic Fe(μ-S)$_2$Fe core are common cofactors in a large number of metalloproteins with various biological functions.[1] Low-molecular weight analogues of such [2Fe–2S] sites with different terminal ligation have been synthesized and investigated thoroughly during the past decades.[2,3] In comparison, much less is known about the structural isomer containing a *trans*-1,2-disulfide-bridged [Fe–S–S–Fe] motif, and only a few examples of it have been structurally characterized.[4,5] Franolic, Millar, and Koch reported that a synthetic [2Fe–2S] precursor with Fe(μ-S)$_2$Fe core can indeed be transformed into an [Fe–S–S–Fe] complex;[4] though not found in nature so far, the latter motif might therefore also be involved in biological transformations of iron–sulfur cofactors. Presented herein are the synthesis and structural and spectroscopic characterizations of an iron tetracarbene dimer bridged by a *trans*-1,2-disulfide. This unusual organometallic compound shows distinct magnetic and spectroscopic properties, and its electronic structure is elucidated with the help of density functional theory (DFT) calculations.

This work originates from the interest of stabilizing bioinorganic key intermediates, including Fe/S-based moieties, by using N-heterocyclic carbene (NHC) ligands.[6] In particular, the macrocyclic tetracarbene ligand L^{TC} [7] has recently enabled the isolation of an unprecedented organometallic oxoiron(IV) complex and of an unusual {FeNO} complex;[8,9] this was achieved by oxo- or NO-transfer onto the iron(II) precursor complex [L^{TC}Fe(MeCN)$_2$](OTf)$_2$ (**1**), which is also starting material for the synthesis of the title compound in this study (Scheme 1). Kühn and co-workers recently reported very similar {FeNO}- and {Fe(CO)$_2$}-tetracarbene complexes employing a derivative of ligand L^{TC} with smaller ring size.[10] Also recently reported was a first NHC-coordinated [M–S–S–M] dimer for M = Ru, with a hydrotris(pyrazolyl)borate and a (2-picolyl)imidazole-2-yliden capping ligand at each metal site.[11]

Scheme 1. Synthesis and Decomposition Pathways of 2

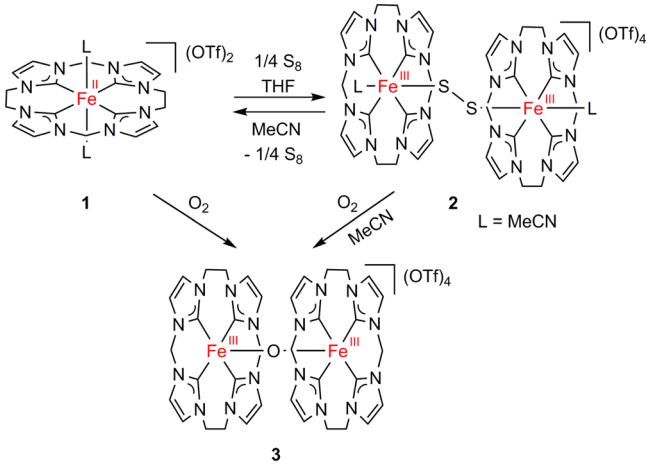

Received: June 26, 2015
Published: October 7, 2015

ACS Publications © 2015 American Chemical Society

DOI: 10.1021/acs.inorgchem.5b01446
Inorg. Chem. 2015, 54, 9770–9776

RESULTS AND DISCUSSION

The reaction of **1** with an excess of elemental sulfur in tetrahydrofuran (THF) produced a dark green precipitate. Purification by slow diffusion of Et_2O into an acetonitrile solution of the dark green crude product at −35 °C gave a brown crystalline material in ∼20% yield. X-ray diffraction of these single crystals identified the product as the disulfide-bridged dinuclear complex **2** (Scheme 1).[12] The low yield results from decomposition of **2** in acetonitrile at ambient temperature to the ferrous starting material **1** and, most probably, elemental sulfur (Scheme 1), suggesting a chemical equilibrium between **1** and **2** in MeCN that is shifting toward **2** the lower the temperature. Polar organic solvents other than MeCN (e.g., acetone, MeOH, dimethylformamide) also lead to decomposition of **2**, while in less polar, noncoordinating solvents (e.g., Et_2O, dichloromethane) **2** is insoluble. Both **1** and **2** are stable at 25 °C under inert conditions in solid state but form, in the presence of dioxygen, the known[8] oxo-bridged tetracarbene iron(III) dimer $[L^{TC}Fe{-}O{-}FeL^{TC}](OTf)_4$ (**3**, Scheme 1) as confirmed by electrospray ionization mass spectrometry (ESI-MS) and UV−vis spectroscopy. The brown crystalline material of **2** was used for all further characterization; however, because of the low solubility and its instability in polar solvents only solid material could be analyzed, and the reactivity of **2** could not be further studied. All attempts to uncover the molecular structure of the green crude material were not successful, mainly hampered by its lability in solution. Nevertheless, close match of the elemental analyses and spectroscopic signatures of the green crude material and the brown crystalline product **2** (Table S1) suggest at least a very similar core structure.

Complex **2** crystallizes in the triclinic space group $P\bar{1}$. The molecular structure reveals a binuclear *trans*-1,2-disulfide-bridged iron tetracarbene complex with four triflate counterions (Figure 1; further bond lengths and angles are listed in Tables S6 and S7).[12] The macrocyclic tetracarbene scaffold provides square-planar basal $\{C_4\}$ ligation,[8,13] and the metal ions are found to be six-coordinate with an MeCN ligand and the bridging disulfide in the axial positions. Altogether, the iron ions exhibit an almost perfect octahedral coordination environment, as apparent from nearly linear S−Fe−N (178.9°) and C−Fe−C angles (174.4° and 175.6°). The Fe−S bond lengths in **2** (2.147 Å) is slightly shorter than those of the above two reference compounds containing a *trans*-1,2-disulfide-bridge (2.191 and 2.163 Å).[4,5] The Fe−C distances in **2** vary between 1.998 and 2.053 Å with short and long bonds trans to each other, alike in the molecular structures of **1** and the μ-oxo tetracarbene iron(III) dimer **3**.[8]

Several binuclear iron complexes with $\mu{-}\eta^1{:}\eta^1$-disulfide bridge have been reported, but most of them feature a *cis*-1,2-disulfide with an additional thiolate[14] or an additional *side-on* $\mu{-}\eta^2{:}\eta^2$-disulfide[15] bridge. According to a Cambridge structural database (CSD) search, only two exclusively *trans*-1,2-disulfide-bridged iron complexes have been characterized by X-ray diffraction so far. One has the [Fe−S−S−Fe] unit capped by tripodal tetradentate $[P(o\text{-}C_6H_4S)_3]^{3-}$ ligands,[4] while the second is coordinated by tetrapodal pentadentate polyamide ligands.[5] The S1−S1′ bond length in **2** (2.023 Å) and in those two related complexes (2.046 and 2.033 Å) are quite similar. Comparison with the S−S bond lengths in H_2S_2 (2.055 Å)[16] and in free S═S (1.887 Å)[17] indicates that all these *trans*-1,2-disulfide-bridged diiron complexes exhibit S−S single-bond

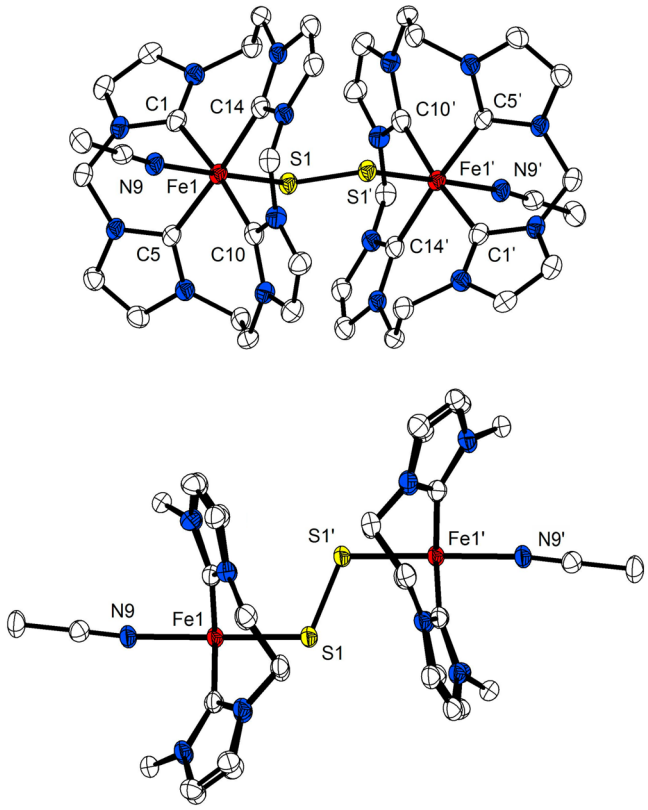

Figure 1. Two different views of the molecular structure of **2** with thermal displacement ellipsoids (shown at 30% probability); hydrogen atoms, solvent molecules, and counterions were omitted for clarity. Symmetry operation used to generate equivalent atoms: (′) $1-x$, $1-y$, $1-z$. Selected bond lengths (Å) and angles (deg): Fe1−C1 1.998(6), Fe1−C5 1.998(5), Fe1−C10 2.053(6), Fe1−C14 2.038(5), Fe1−S1 2.1475(16), Fe1−N9 1.993(5), S1−S1′ 2.023(3); N9−Fe1−S1 178.95(15), C1−Fe1−C10 174.4(2), C5−Fe1−C14 175.6(2), C1−Fe1−S1 90.49(17), C5−Fe1−S1 91.35(15), C10−Fe1−S1 92.81(17), C14−Fe1−S1 91.42(16), S1−S1′−Fe1 112.59(9).[12]

character. Generally, binuclear *trans*-1,2-disulfide-bridged complexes can be formally described by three resonance structures (Scheme 2) with different metal oxidation states and S_2^{2-} (**I**), S_2^{-} (**II**), or S_2 bridge (**III**);[14b] the structural data support the presence of ferric ions in **2**.

Scheme 2. Resonance Structures for the Fe−($\mu{-}\eta^1{:}\eta^1$-S_2)−Fe core of 2[14b]

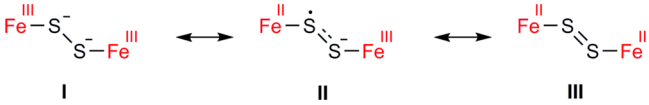

Resonance Raman spectroscopy (λ_{ex} = 633 nm) of **2** shows two relatively intense new bands in comparison with the mononuclear ferrous complex **1** and μ-oxo diferric complex **3** (Figure 2), which were assigned to the symmetric υ_{Fe-S} (at 389 cm^{-1}) and υ_{S-S} (at 501 cm^{-1}) stretching modes; as expected, these totally symmetric (A_g) vibrations are not observed in the IR spectrum (Figure S1). Furthermore, these frequencies are in good agreement with the DFT-calculated ones for the υ_{Fe-S} and υ_{S-S} stretches of **2** (379 and 483 cm^{-1}, respectively). A *trans*-1,2 end-on disulfide bridged dicopper(II) complex showed a very similar υ_{S-S} stretch at 499 cm^{-1},[18] while values for some [Ru−

DOI: 10.1021/acs.inorgchem.5b01446
Inorg. Chem. 2015, 54, 9770−9776

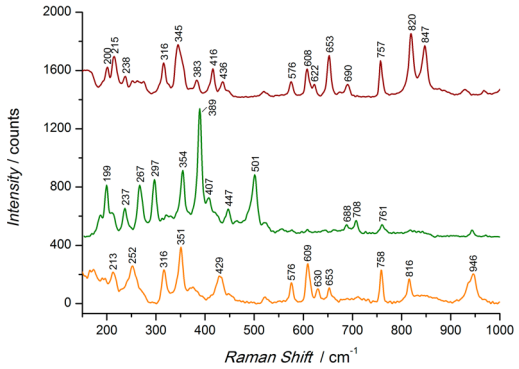

Figure 2. Raman spectra (λ_{ex} = 633 nm) of **1** (lower; orange spectrum), **2** (middle; green spectrum), and **3** (upper; brown spectrum) in the region between 150 and 1000 cm^{-1} recorded at room temperature.

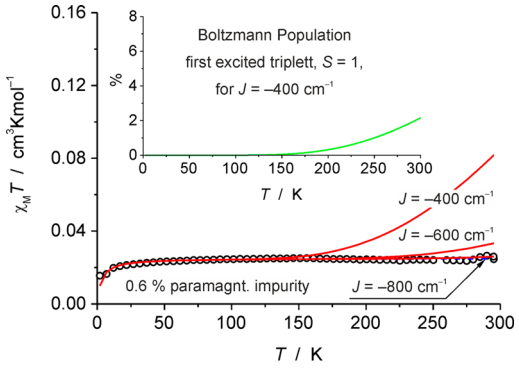

Figure 3. Temperature dependence of the magnetic susceptibility for **2** recorded with B = 0.5 T applied field (○) and spin-Hamiltonian simulations with spins $S_1 = S_2 = 1/2$ and different J values. Since only the first excited state with total spin S = 1 is found to be populated by not more than 2% at 295 K, as shown in the inset, identical results are obtained for S_i = 3/2, 2, and 5/2. The experimental data were corrected for a constant TIP-like contribution to χ of 540 × 10^{-6} cm^3 mol^{-1}, and a minor paramagnetic impurity of 0.6% with S = 5/2 was included in the simulations to account for the data offset.

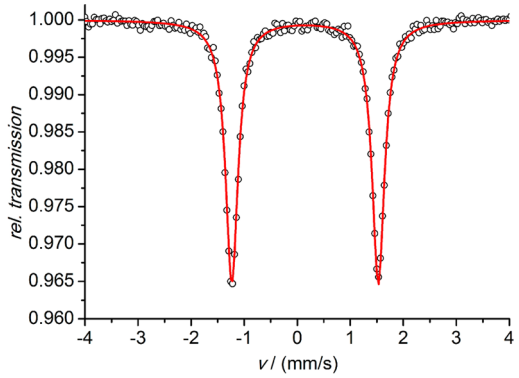

Figure 4. Zero-field Mössbauer spectrum of crystalline **2** at 80 K. The solid line represents the calculated Lorentzian doublet.

S−S−Ru] complexes were found at slightly higher energies (~530 cm^{-1}).[19,20] Surprisingly, the IR spectrum of **2** does not reveal any sharp absorption bands in the range of 2200−2300 cm^{-1} typical for C≡N modes[21] (Figure S1c), even though MeCN is clearly present in the molecular structure. In comparison, the IR spectrum of **1** shows a C≡N stretching band at 2258 cm^{-1} originating from its two axial MeCN ligands (Figure S1c). However, the IR spectrum of a related structurally authenticated iron(II) complex with a macrocyclic N-heterocyclic carbene/pyridine hybrid ligand and two MeCN in axial positions showed no C≡N stretching mode despite being structurally very similar to **1**.[22] DFT calculations of the IR spectra revealed the presence of a C≡N stretching band at 2231 cm^{-1} for **1** (close to the experimental value of 2258 cm^{-1}) and at 2257 cm^{-1} for **2**, but the signal intensity for **2** was calculated to be rather weak compared to **1** (Figure S4). We therefore conclude that the coordination of certain ligands to the iron center, for example, Fe−S or Fe−N_{py}, may effect vibrational quenching of the C≡N mode of coordinated MeCN in these systems. In the case of **2** the C≡N stretching band is presumably fading into the background noise.

Magnetic susceptibility data for **2**, collected in the temperature range from 2 to 295 K, show essentially diamagnetic behavior up to room temperature. Simulations using the Hamiltonian $\hat{H} = -2JS_1S_2$ indicate an extremely strong antiferromagnetic coupling of the local iron sites with $-J$ > 800 cm^{-1}, resulting in a well-separated S = 0 ground state and at most minute population of the first excited state with S = 1 (Figure 3). Therefore, according to the general "spin ladder" rule for dimers, $E(S) = J\,S(S+1) + constant$, any symmetric pair of local spins S_i = 1/2, 3/2, or 5/2 for iron(III) would be consistent with the data, but also iron(II) with S_i = 2, and even S_i = 0 could not be readily excluded here. Hence, like in the case of the μ-oxo diiron(III) complex **3** ($-J$ = 606 cm^{-1}),[8] iron oxidation states unfortunately cannot be determined from the susceptibility measurement. No magnetic data of other exclusively *trans*-1,2-disulfide-bridged diiron complexes are available for comparison of the strong exchange coupling constant J.

Zero-field ^{57}Fe Mössbauer spectroscopy of **2** shows a single quadrupole doublet with isomer shift δ = 0.15 mm/s and quadrupole splitting ΔE_Q = 2.76 mm/s at 80 K (Figure 4). The unique spectrum reveals essentially identical local iron sites and, thus, argues against the mixed-valence configuration (**II**; Scheme 2). Moreover, applied-field measurements in consistency with the susceptibility data show the absence of internal fields at the iron nuclei, corroborating the diamagnetic behavior and singlet ground state of **2**. Simulations of the spectra disclose a positive sign for the electric field gradient at the ^{57}Fe nuclei, with a moderately strong asymmetry parameter η = 0.7 (Figure S2).

The observation that the isomer shift of **2** (0.15 mm/s) is significantly lower than δ = 0.23 mm/s found for the low-spin ferrous parent complex **1** with a similar bonding pattern[8] suggests that **2** is a ferric low-spin compound, which will be substantiated by DFT calculations given below. Heuristically, the difference can be rationalized also by the higher covalence of the iron−sulfur bonds of **2**, which correlates with low isomer shifts, compared to O and N ligands, as found for all Fe/S clusters.[2] The relatively large quadrupole splitting of **2** is consistent with the low-spin diferric state, due to the strong valence contribution to the electric field gradient expected for a $3d^5$ low-spin configuration with strong d-charge anisotropy around the iron nuclei. In detail, however, the balance of covalent bonds arising from the strong σ interaction of the equatorial tetracarbene ligand and the axial S and N ligands also has strong influence, as can be inferred below from the DFT results. Similar large quadrupole splitting therefore was also observed for the other iron tetracarbene complexes of L^{TC} in

DOI: 10.1021/acs.inorgchem.5b01446
Inorg. Chem. 2015, 54, 9770−9776

the metal oxidation states +II (**1**), +III (**3**), and +IV (Fe^{IV}=O complex),[8] as well as for the related iron(II) and iron(III) complexes of a macrocyclic N-heterocyclic carbene/pyridine hybrid ligand.[22]

We mention that comparable Mössbauer data are available for only one other complex with a *trans*-1,2-disulfide-bridge, namely, for the $[Fe_2(\mu\text{-}S_2)(P(o\text{-}C_6H_4S)_3)_2]^{2-}$ anion with tetradentate $\{S_3P\}$ capping ligands and five-coordinate iron sites showing δ = 0.35 mm/s and ΔE_Q = 2.04 mm/s.[4] Although not explicitly assigned there, the isomer shift is more common for iron(III) in high-spin state;[23] in particular, it compares quite well with those of the tetrahedral ferric sites in typical iron−sulfur clusters with $\delta \approx 0.3$ mm/s.[3a,24] The relatively large quadrupole splitting of $[Fe_2(\mu\text{-}S_2)(P(o\text{-}C_6H_4S)_3)_2]^{2-}$ does not contradict the interpretation as high-spin ferric compound because the asymmetric bipyramidal five-coordination with a phosphorus atom and the −S−S− bridging ligand in apical positions may induce sizable asymmetry of the covalent bonds around the metal ion. In such case, the ferric high-spin ions can show large quadrupole splitting, arising from the highly asymmetric ligand environment,[23] although the formally uniform $3d^5$ population (in a crystal field model) affords no valence contribution to the electric field gradient. Classical examples are the oxo-bridged Fe^{III}−O−Fe^{III} centers encountered in diiron enzymes like ribonucleotide reductase and related model compounds,[25] for which the single "unbalanced", highly covalent oxo bond can induce large quadrupole splitting, up to ΔE_Q = 2.45 mm/s.[25a,c]

The Mössbauer parameters of **2** resemble those of the diferric μ-oxo complex **3** (δ = 0.04 mm/s, ΔE_Q = 2.56 mm/s),[8] the local electron configuration of which was recently experimentally assigned to low-spin iron(III), based on a heuristic correlation of the isomer shift with the formal oxidation state for three complexes with the same tetracarbene ligand L^{TC}.[8] This unusual assignment, however, must be revised in view of the present DFT results (see below).

Solid-state UV−vis−NIR (NIR = near-IR) spectroscopy of **2** revealed absorption bands in the UV (~360 nm), visible (682 nm), and near-IR (1015 nm) regions (Figure 5). Broad and

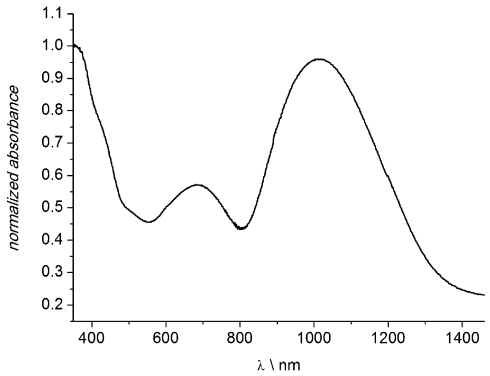

Figure 5. Solid-state UV−vis−NIR spectrum of **2** measured in KBr powder.

intense NIR bands are characteristic for binuclear *trans*-1,2-disulfide complexes of ruthenium and iron. Sellmann and coworkers assigned them to $\pi \rightarrow \pi^*$ transitions of the delocalized 4-center-6-electron [M−S−S−M] core.[19,26] On the basis of TD-DFT calculations (B3LYP/def2-TZVP/RIJCOSX/COSMO) the band at 1015 nm for **2** (calculated λ_{max} = 872 nm) can now be assigned to a S → Fe LMCT transition (see Figure S3 for details). In the case of the *trans*-1,2 end-on disulfide bridged dicopper(II) complex and some related diruthenium complexes the NIR bands were found at significantly higher energies (586 nm and 700−800 nm, respectively),[18−20,26,27] reflecting the lower-lying Fe-based lowest unoccupied molecular orbital in the ferric case.

To corroborate the spectroscopic assignments and to finally elucidate the electronic structure of **2**, DFT calculations were performed based on the molecular structure determined by X-ray diffraction, assuming different spin states and coupling schemes (Table 1; for more extended data see Table S2). Broken-symmetry DFT calculations were attempted starting from different assumptions for the number of unpaired electrons on each center. As in previous work[28] the notation BS(m,n) corresponds to a broken symmetry starting wave function with n unpaired "spin up" electrons on the "left" and m unpaired "spin down" electrons on the "right" side of the complex. Optimization of BS(0,0) (corresponding to low-spin Fe^{II} centers), BS(1,1) (corresponding to low-spin Fe^{III} centers), BS(2,2) (corresponding to intermediate spin Fe^{II} centers), BS(3,3) (corresponding to intermediate spin Fe^{III} centers), BS(4,4) (corresponding to high spin Fe^{II} centers), and BS(5,5) (corresponding to high-spin Fe^{III} centers) were attempted. Only two distinct solutions were found, which are the ground-state configuration BS(1,1) and a much higher-energy solution BS(5,5), as shown in Table 1. Attempts to converge to BS(2,2), BS(3,3), and BS(4,4) always resulted in the same BS(1,1) solution. The high energy of the BS(5,5) solution, in contrast, is plausible since the strong in-plane tetracarbene ligand should destabilize the $d_{x^2-y^2}$ orbital and make the local high-spin configuration unfavorable. Optimization of the broken-symmetry geometry for BS(1,1) did not change the picture. The calculated J value at the optimized geometry is −836 cm^{-1}, that is, the same as at the high-spin geometry. Also calculated Mössbauer parameters agree reasonably well with experiment (Tables 1 and S2), as well as the metric details of the calculated molecular structure (Table S3). Loewdin spin-populations are found at 0.75/−0.75 on iron and 0.14/−0.14 on sulfur (for more details see Table S2). Hence, on the basis of the calculations and the agreement between calculated and experimental Mössbauer parameters and exchange coupling, the ground state of the complex is best viewed as featuring two low-spin iron(III) centers with strong antiferromagnetic coupling via a S_2^{2-} bridging unit. The orbital scheme (Figure 6) shows that the coupling proceeds via the d_{xz} magnetic orbitals that mix with sulfur p_x orbitals. The d_{xy} and d_{yz} orbitals are doubly occupied, while the d_{z^2} and $d_{x^2-y^2}$ orbitals are vacant. In the literature six-coordinate iron(III) low-spin $O^{2-}/O_2^{2-}/S^{2-}/S_2^{2-}$-bridged dimers are rare. This unusual ground state has been found for a set of phthalocyaninato μ-oxo diiron(III) complexes,[29] but the antiferromagnetic coupling in those complexes ($-J$ < 10 cm^{-1}) is 2 orders of magnitude smaller than in **2**.

For comparison, the electronic structure of the oxo-bridged complex **3**[8] was also explored by broken-symmetry analyses as described above. In contrast to the low-spin situation encountered with **2**, for compound **3** the best agreement of calculated spin coupling constants with experiment is found for the BS(3,3) solution, which corresponds to antiferromagnetic coupling of two ferric centers with intermediate spin S_i = 3/2 (for details see Table S4). Note that **2** and **3** differ by the lack of axial MeCN ligands in the latter, significantly stabilizing the

DOI: 10.1021/acs.inorgchem.5b01446
Inorg. Chem. 2015, 54, 9770−9776

Table 1. Relative Energies, Exchange Coupling Constants J, Mössbauer Isomer Shifts δ, Quadrupole Interaction Parameters ΔE_Q, η, and Loewdin Spin-Populations of Closed-Shell and Various Open-Shell Configurations of 2 Calculated by DTF on the Basis of the X-ray Molecular Structure

	E^{rel}	J	δ	ΔE_Q	η[a]	Loewdin spin-population			
	kJ mol	cm^{-1}	mm/s	mm/s		Fe	S	S	Fe
$S = 0$	46	0	0.15	2.55	0.72	0.00	0.00	0.00	0.00
BS(1,1)	0	−912	0.10	−2.93[b]	0.94	0.75	0.14	−0.14	−0.75
BS(5,5)	548	−836	0.16	−0.97	0.68	3.80	0.25	−0.25	−3.80
opt BS(1,1)		−836	0.07	−2.78[b]	0.97	0.76	0.14	−0.14	−0.76
experimental		<−800	0.15	2.78	0.72				

[a]Asymmetry parameter of the electric field gradient. [b]The sign of the quadrupole splitting is physically insignificant here because of the large calculated value of the asymmetry η close to 1, for which the electric field gradient tensor has essentially two equally large components of opposite sign.[23]

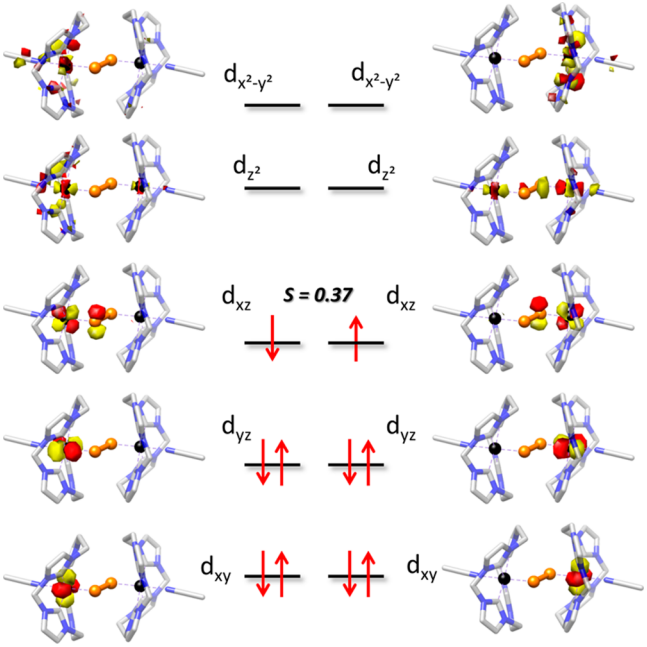

Figure 6. Orbital scheme from localized quasi-restricted orbitals (doubly occupied), magnetic orbitals (overlap $S = 0.37$), and quasi-restricted orbitals (vacant orbitals) for the BS(1,1) configuration of **2**. Hydrogen atoms are omitted for clarity.

d_{z^2} orbitals for the five-coordinate ferric ions in **3**. A plot of the molecular orbitals reveals that the strong antiferromagnetic coupling proceeds via the magnetic d_{xz}, d_{yz}, and d_{z^2} orbitals (Figure S5). Since also the experimental Mössbauer parameters of **3** could be well-reproduced by the BS(3,3) solution, and optimization of the structure in this spin-state as well resulted in very good agreement with the X-ray structure, we must revise our previous empirical assignment of **3** as a diferric low-spin complex.[8] In view of the DFT results the oxo-bridged dimer has intermediate local spins $S_i = 3/2$.

CONCLUSIONS

A detailed structural, spectroscopic, and computational study has revealed that the novel tetracarbene-ligated diiron complex $[L^{TC}(MeCN)Fe-S-S-Fe(MeCN)L^{TC}](OTf)_4$ (**2**) is best described as a diferric system with S_2^{2-} bridge and with S−S single bond character. The NIR band typical for such systems with [Fe−S−S−Fe] core has been assigned to a S→Fe LMCT transition, and a low-spin state of the iron(III) ions with extremely strong antiferromagnetic coupling has been established. The electronic ground state of the herein-presented [Fe−S−S−Fe] complex originates from the very strong σ-donor tetracarbene ligation, which raises the iron $d_{x^2-y^2}$ orbital and, together with the axial disulfide, leads to large separation of the e_g and t_{2g} orbital sets. In contrast, the oxo-bridged ferric dimer $[L^{TC}Fe-O-FeL^{TC}]^{4+}$ (**3**) with five-coordinate metal ions has intermediate local spins $S_i = 3/2$. Finally, note that the corresponding oxo analogue of the new disulfido complex $[L^{TC}(MeCN)Fe-S-S-Fe(MeCN)L^{TC}]^{4+}$ is a mononuclear oxoiron(IV) complex $[L^{TC}(MeCN)Fe{=}O]^{2+}$ instead of a dimeric 1,2-peroxo diiron(III) species $[L^{TC}(MeCN)Fe-O-O-Fe(MeCN)L^{TC}]^{4+}$ akin to **2**.[8]

EXPERIMENTAL SECTION

General. All reactions were performed under dry argon using standard Schlenk techniques, or in a glovebox (MBRAUN LabMaster) under nitrogen atmosphere with less than 0.1 ppm of O_2 and H_2O. Solvents were dried and degassed by standard procedures before use. Chemicals were purchased from commercial sources and used as received. Complex **1** was prepared according to literature.[8] Solid-state UV−vis−NIR spectra were collected with a Varian Cary 5000 instrument using a praying mantis sampling kit for diffuse reflection. Raman spectra were recorded using a HORIBA Scientific LabRAM HR 800 (400−1100 nm) spectrometer with open electrode CCD detector and a confocal pinhole with user controlled variable aperture in combination with a free space optical microscope and a He:Ne laser with an excitation at 632.8 nm. Solid-state AT-IR measurements were performed with a Cary 630 FTIR spectrometer under inert conditions in a glovebox and analyzed by FTIR MicroLab software.

Synthesis of Complex 2. To a suspension of **1** (50 mg, 0.071 mmol, 1.00 equiv) in THF (3 mL) was added a solution of freshly sublimated S_8 (6.8 mg, 0.21 mmol, 3.0 equiv) in THF (2 mL). The reaction mixture was stirred at ambient temperature overnight. The precipitate was separated by filtration and washed with THF (2 × 3 mL). Removal of the solvent under vacuum gave a dark green powder. Brown single crystals of **2** suitable for X-ray diffraction were grown by slow diffusion of Et_2O into an MeCN solution of the green product at −35 °C with a yield of ∼20% (11 mg, 7.1 μmol). mp ≈ 150 °C (dec).[12] UV−vis−NIR (solid, KBr): λ_{max} [nm]: ∼360, 682, 1015. ATR-IR: $\tilde{\nu}$ (cm^{-1}) = 3180 (w), 3135 (w), 3110 (w), 1589 (w), 1574 (w), 1480 (w), 1457 (w), 1405 (m), 1334 (w), 1275 (m), 1245 (s), 1222 (m), 1152 (m), 1118 (m), 1062 (w), 1025 (s), 965 (w), 935 (w), 812 (w), 757 (m), 742 (m), 701 (m), 686 (m), 637 (s), 574 (m), 514 (s), 462 (w). Anal. Calcd (%) for $C_{44}H_{46}F_{12}Fe_2N_{18}O_{12}S_6$: C 34.07, H 2.99, N 16.26, S 12.40. Found: C 34.42, H 3.35, N 15.83, S 12.34.

Mössbauer Spectroscopy. Zero-field Mössbauer spectra were recorded with a ^{57}Co source in a Rh matrix using an alternating constant-acceleration Wissel Mössbauer spectrometer operated in transmission mode and equipped with a Janis closed-cycle helium cryostat, whereas applied-field measurements were performed in an Oxford Instruments Mössbauer-Spectromag split-pair magnet system

DOI: 10.1021/acs.inorgchem.5b01446
Inorg. Chem. 2015, 54, 9770−9776

with the field at the sample being oriented perpendicular to the γ-beam. The γ-source (^{57}Co/Rh, 1.8 GBq) was kept at room temperature. By using a re-entrant bore tube the γ-source could be positioned inside the gap of the magnet coils at a position with zero field. Isomer shifts are quoted relative to iron metal at 300 K.

Magnetic Susceptibility Measurement. Temperature-dependent magnetic susceptibilities were measured by using a SQUID magnetometer (Quantum Design MPMS XL-5). The powdered sample was contained in a gel bucket and fixed in a nonmagnetic sample holder. Each raw data file for the measured magnetic moment was corrected for the diamagnetic contribution of the sample holder and the gel bucket. The molar susceptibility data were corrected for the diamagnetic contribution. Magnetic properties were simulated using the julX program.[30] Temperature-independent paramagnetism (TIP) and paramagnetic impurities (PI) with $S = 5/2$ and a Weiss constant $\Theta = -3$ K (accounting for intermolecular interactions) were included according to $\chi_{calc} = (1 - PI)\cdot\chi + PI\cdot\chi_{mono} + TIP$ (TIP = 540 $\times 10^{-6}$ cm^3 mol^{-1}, PI = 0.6%) for **2**.

X-ray Crystallography. X-ray data were collected on a STOE IPDS II diffractometer with an area detector (graphite monochromated Mo−Kα radiation, λ = 0.710 73 Å) by use of ω scans at 133 K (Table S4). The structure was solved by direct methods and refined on F^2 with all reflections using SHELXL-14.[31] Non-hydrogen atoms were refined anisotropically. Hydrogen atoms were placed in calculated positions and assigned to an isotropic displacement parameter of 1.2/1.5 U_{eq}(C). Face-indexed absorption corrections were performed numerically with the program X-RED.[32] Crystal and refinement data are collected in Table S2. Additional crystallographic information is available in the Supporting Information.

Computational Methodology. All calculations were performed with the ORCA[33] program. Energies and spectroscopic parameters were calculated with the B3LYP functional[34] in conjunction with the RIJCOSX[35] approximation, the def2-TZVP basis set, and the corresponding def2-TZV/J auxiliary basis set.[36] For the Mössbauer calculation the CP(PPP)[37] basis set was used for iron. Structure optimization was performed with the BP86[38] functional, the resolution of the identity approximation (RI),[39] a def2-TZVP[36] basis set, and the def2-TZVP/J auxiliary basis set. The resulting structure was verified as a local minimum on the potential energy surface by numerical frequency calculation, which resulted in only positive normal vibrations. For all calculations solvent effects were taken into account by the conductor-like screening model (COSMO)[40] considering acetonitrile as solvent.

■ ASSOCIATED CONTENT

Supporting Information

The Supporting Information is available free of charge on the ACS Publications website at DOI: 10.1021/acs.inorgchem.5b01446. CCDC-1055956 (**2**) contains the supplementary crystallographic data for this paper. These data can be obtained free of charge from The Cambridge Crystallographic Data Centre via http://www.ccdc.cam.ac.uk/data_request/cif.

Tabulated analytical data for comparing crude product **2** to crystallized product **2**, AT-IR spectra, Mossbauer spectra, DFT calculational details, optimized geometric parameters, calculated UV−vis−NIR absorption spectrum, variouis parameters for different spin states, illustrated molecular orbital scheme from calculations, tabulated crystal data, refinement details, and bond lengths and angles. (PDF)

X-ray crystallographic data. (CIF)

■ AUTHOR INFORMATION

Corresponding Authors

*E-mail: Frank.Neese@cec.mpg.de. (F.N.)

*E-mail: franc.meyer@chemie.uni-goettingen.de. (F.M.)

Author Contributions

The manuscript was written through contributions of all authors. All authors have given approval to the final version of the manuscript.

Notes

The authors declare no competing financial interest.

■ ACKNOWLEDGMENTS

Financial support by the DFG (International Research Training Group IRTG 1422 “Metal Sites in Biomolecules: Structures, Regulation and Mechanisms”) and the Fonds der Chemischen Industrie (Kekulé fellowship for C.K.) is gratefully acknowledged.

■ DEDICATION

Dedicated to Prof. Herbert W. Roesky on the occasion of his 80th birthday.

■ REFERENCES

(1) *Handbook of Metalloproteins;* Messerschmidt, A., Huber, R., Poulos, T., Wieghardt, K., Eds.; John Wiley & Sons: Chichester, 2001; Vols. *1 & 2*.

(2) Rao, P. V.; Holm, R. H. *Chem. Rev.* **2004**, *104*, 527.

(3) (a) Ballmann, J.; Albers, A.; Demeshko, S.; Dechert, S.; Bill, E.; Bothe, E.; Ryde, U.; Meyer, F. *Angew. Chem., Int. Ed.* **2008**, *47*, 9537. (b) Albers, A.; Demeshko, S.; Dechert, S.; Saouma, C. T.; Mayer, J. M.; Meyer, F. *J. Am. Chem. Soc.* **2014**, *136*, 3946.

(4) Franolic, J. D.; Millar, M.; Koch, S. A. *Inorg. Chem.* **1995**, *34*, 1981.

(5) Kämpf, H.; Daunke, D.; Heinemann, F. W.; Grohmann, A. *Appl. Phys. A: Mater. Sci. Process.* **2008**, *93*, 303.

(6) (a) Liu, T.; Darensbourg, M. Y. *J. Am. Chem. Soc.* **2007**, *129*, 7008. (b) Deng, L.; Holm, R. H. *J. Am. Chem. Soc.* **2008**, *130*, 9878. (c) Scepaniak, J. J.; Vogel, C. S.; Khusniyarov, M. M.; Heinemann, F. W.; Meyer, K.; Smith, J. M. *Science* **2011**, *331*, 1049.

(7) Bass, H. M.; Cramer, S. A.; Price, J. L.; Jenkins, D. M. *Organometallics* **2010**, *29*, 3235.

(8) Meyer, S.; Klawitter, I.; Demeshko, S.; Bill, E.; Meyer, F. *Angew. Chem., Int. Ed.* **2013**, *52*, 901.

(9) Kupper, C.; Schober, A.; Demeshko, S.; Bergner, M.; Meyer, F. *Inorg. Chem.* **2015**, *54*, 3096.

(10) Anneser, M. R.; Haslinger, S.; Pöthig, A.; Cokoja, M.; Basset, J.-M.; Kühn, F. E. *Inorg. Chem.* **2015**, *54*, 3797.

(11) Fernandez, F. E.; Puerta, M. C.; Valerga, P. *Inorg. Chem.* **2013**, *52*, 4396.

(12) Meyer, S. *Bioinspired Organometallic Analogues of Iron-Sites in Metalloproteins*, Dissertation, Cuvillier Verlag: Göttingen, Germany, 2015.

(13) Cramer, S. A.; Jenkins, D. M. *J. Am. Chem. Soc.* **2011**, *133*, 19342.

(14) for examples see: (a) Terzis, A.; Rivest, R. *Inorg. Chem.* **1973**, *12*, 2132. (b) Kubas, G. T.; Spiro, T. G.; Terzis, A. *J. Am. Chem. Soc.* **1973**, *95*, 273. (c) Vergamini, P. J.; Ryan, R. R.; Kubas, G. J. *J. Am. Chem. Soc.* **1976**, *98*, 1980. (d) Sellmann, D.; Mahr, G.; Knoch, F. *Angew. Chem., Int. Ed. Engl.* **1991**, *30*, 1477.

(15) for examples see: (a) Weberg, R.; Haltiwanger, R. C.; DuBois, M. R. *Organometallics* **1985**, *4*, 1315. (b) Brunner, H.; Janietz, N.; Meier, W.; Sergeson, G.; Wachter, J.; Zahn, T.; Ziegler, M. L. *Angew. Chem., Int. Ed. Engl.* **1985**, *24*, 1060.

(16) Winnewisser, G.; Winnewisser, M.; Gordy, W. *J. Chem. Phys.* **1968**, *49*, 3465.

(17) Müller, A.; Jagermann, W. *Inorg. Chem.* **1979**, *18*, 2631.

(18) Chen, P.; Fujisawa, K.; Helton, M. E.; Karlin, K. D.; Solomon, E. I. *J. Am. Chem. Soc.* **2003**, *125*, 6394.

(19) Sellmann, D.; Lechner, P.; Knoch, F.; Moll, M. *J. Am. Chem. Soc.* **1992**, *114*, 922.

DOI: 10.1021/acs.inorgchem.5b01446
Inorg. Chem. 2015, 54, 9770−9776

(20) Amarasekera, J.; Rauchfuss, T. B.; Wilson, S. R. *Inorg. Chem.* **1987**, *26*, 3328.
(21) Nakamoto, K. *Infrared Spectra in Inorganic and Coordination Compounds;* John Wiley & Sons: Hoboken, NJ, 1970.
(22) Klawitter, I.; Anneser, M. R.; Dechert, S.; Meyer, S.; Demeshko, S.; Haslinger, S.; Pöthig, A.; Kühn, F. E.; Meyer, F. *Organometallics* **2015**, *34*, 2819.
(23) Gütlich, P.; Bill, E.; Trautwein, A. X. *Mössbauer Spectroscopy and Transition Metal Chemistry;* Springer: Heidelberg, 2011.
(24) (a) Schünemann, V.; Winkler, H. *Rep. Prog. Phys.* **2000**, *63*, 263. (b) Bill, E. *Hyperfine Interact.* **2012**, *205*, 139. (c) Ballmann, J.; Sun, X. R.; Dechert, S.; Bill, E.; Meyer, F. *J. Inorg. Biochem.* **2007**, *101*, 305. (d) Albers, A.; Demeshko, S.; Dechert, S.; Bill, E.; Bothe, E.; Meyer, F. *Angew. Chem., Int. Ed.* **2011**, *50*, 9191.
(25) (a) Atkin, C. I.; Thelander, L.; Reichhard, P.; Lang, G. *J. Biol. Chem.* **1973**, *248*, 7464. (b) Vincent, J. B.; Olivier-Lilley, G. L.; Averill, B. A. *Chem. Rev.* **1990**, *90*, 1447. (c) Kurtz, D. M. *Chem. Rev.* **1990**, *90*, 585.
(26) (a) Sellmann, D.; Barth, I. *Inorg. Chim. Acta* **1989**, *164*, 171. (b) Sellmann, D.; Mahr, G.; Knoch, F. *Angew. Chem., Int. Ed. Engl.* **1991**, *30*, 1477.
(27) Schneider, R.; Wieghardt, K.; Nuber, B. *Inorg. Chem.* **1993**, *32*, 4935.
(28) Bart, S. C.; Chlopek, K.; Bill, E.; Bouwkamp, M. W.; Lobkovsky, E.; Neese, F.; Wieghardt, K.; Chirik, P. J. *J. Am. Chem. Soc.* **2006**, *128*, 13901.
(29) (a) Ercolani, C.; Gardini, M.; Murray, K. S.; Pennesi, G.; Rossi, G.; Zwack, P. R. *Inorg. Chem.* **1987**, *26*, 3539. (b) Bakshi, E. N.; Murray, K. S. *Hyperfine Interact.* **1988**, *40*, 283.
(30) Bill, E. *julX;* Max-Planck Institute for Chemical Energy Conversion: Mülheim/Ruhr, Germany.
(31) Sheldrick, G. M. *Acta Crystallogr., Sect. A: Found. Crystallogr.* **2008**, *A64*, 112.
(32) *X-RED;* STOE & CIE GmbH: Darmstadt, Germany, 2002.
(33) Neese, F. *WIREs Comput. Mol. Sci.* **2012**, *2*, 73. The ORCA program is available free of charge at www.cec.mpg.de/downloads.html.10.1002/wcms.81
(34) (a) Lee, C. T.; Yang, W. T.; Parr, R. G. *Phys. Rev. B: Condens. Matter Mater. Phys.* **1988**, *37*, 785. (b) Becke, A. D. *J. Chem. Phys.* **1993**, *98*, 5648.
(35) Neese, F.; Wennmohs, F.; Hansen, A.; Becker, U. *Chem. Phys.* **2009**, *356*, 98.
(36) (a) Schafer, A.; Horn, H.; Ahlrichs, A. *J. Chem. Phys.* **1992**, *97*, 2571. (b) Weigend, F.; Ahlrichs, R. *Phys. Chem. Chem. Phys.* **2005**, *7*, 3297.
(37) Neese, F. *Inorg. Chim. Acta* **2002**, *337*, 181.
(38) (a) Becke, A. D. *Phys. Rev. A: At., Mol., Opt. Phys.* **1988**, *38*, 3098. (b) Perdew, J. P. *Phys. Rev. B: Condens. Matter Mater. Phys.* **1986**, *34*, 7406. (c) Perdew, J. P. *Phys. Rev. B: Condens. Matter Mater. Phys.* **1986**, *33*, 8822.
(39) Vahtras, O.; Almlof, J.; Feyereisen, M. W. *Chem. Phys. Lett.* **1993**, *213*, 514.
(40) (a) Klamt, A.; Schuurmann, G. *J. Chem. Soc., Perkin Trans. 2* **1993**, 799. (b) Klamt, A. *J. Phys. Chem.* **1995**, *99*, 2224.

DOI: 10.1021/acs.inorgchem.5b01446
Inorg. Chem. 2015, 54, 9770−9776